Mechanically tunable metamaterials terahertz dual-band bandstop filter*

Fangrong Hu(胡放荣)[1,3,†], Xin Xu(胥欣)[1], Peng Li(李鹏)[1], Xinlong Xu(徐新龙)[2], and Yue'e Wang(王月娥)[1]

[1] *Guangxi Colleges and Universities Key Laboratory of Optoelectronic Information Processing, Guilin University of Electronic Technology, Guilin* 541004, *China*

[2] *Nanobiophotonic Center, State Key Laboratory Incubation Base of Photoelectric Technology and Functional Materials, and Institute of Photonics & Photon-Technology, Northwest University, Xi'an* 710069, *China*

[3] *Guangxi Experiment Center of Information Science, Guilin University of Electronic Technology, Guilin* 541004, *China*

(Received 12 January 2017; revised manuscript received 24 March 2017; published online 6 June 2017)

We experimentally demonstrate a mechanically tunable metamaterials terahertz (THz) dual-band bandstop filter. The unit cell of the filter contains an inner aluminum circle and an outside aluminum Ohm-ring on high resistance silicon substrate. The performance of the filter is simulated by finite-integration-time-domain (FITD) method. The sample is fabricated using a surface micromachining process and experimentally demonstrated using a THz time-domain-spectroscopy (TDS) system. The results show that, when the incident THz wave is polarized in *y*-axis, the filter has two intensive absorption peaks locating at 0.71 THz and 1.13 THz, respectively. The position of the high-frequency absorption peak and the amplitude of the low-frequency absorption peak can be simultaneously tuned by rotating the sample along its normal axis. The tunability of the high-frequency absorption peak is due to the shift of resonance frequency of two electrical dipoles, and that of the low-frequency absorption peak results from the effect of rotationally induced transparent. This tunable filter is very useful for switch, manipulation, and frequency selective detection of THz beam.

Keywords: metamaterials, terahertz (THz) bandstop filter, mechanically tunable, rotationally induced transparent (RIT)

PACS: 42.79.Ci, 81.05.Xj, 84.30.Vn **DOI:** 10.1088/1674-1056/26/7/074219

1. Introduction

Generally, the frequency of terahertz (THz) radiation lies between 0.1 and 10 THz region.[1] THz spectroscopy has many excellent features, such as better penetrability, good security, distinctive fingerprint spectrum of many substances, and so on. Therefore, it has potential applications in the field of security checking,[2] bio-medicine,[3] substance identification,[4] and product quality monitoring.[5] At present, due to a lack of high-efficiency radiation source, high-sensitivity detector, and many other functional devices, it is still a challenge for wide applications of THz technology.

Metamaterials[6–8] are artificially constructed electromagnetic (EM) materials and structures which have many exotic EM performances. Therefore, they can be used to construct some new devices and have been applied in many fields. Until now, many metamaterial-based devices, such as emitters,[9] detectors,[10] and absorbers,[11–14] have been presented and demonstrated in the THz region.

The filter[15] is an important device for manipulating the THz beam. So far, various THz filters based on metamaterials (MMs)[16–19] have been investigated. With the rapid development of THz technology, the demand for high-performance tunable THz filters is increasing. Recently, mechanically tunable bandstop filters based on metamaterials and microelectromechanical systems (MEMS) technology have attracted tremendous interest. Ozbey[20] numerically demonstrated magnetic-film-based cantilevers for continuously tuning over a large frequency range of 0.3 THz. By changing the relative distance between two split-ring resonators, Fu *et al.*[21] proposed a THz filter with a tunable frequency range about 0.2 THz. Li *et al.*[22] demonstrated a THz metamaterial bandstop filter comprising an array of identical subwavelength resonators, each consisting of a pair of printable metallic U-shapes that have their openings pointing in opposite directions. Prakash[23] experimentally demonstrated a MEMS reconfigurable metamaterial with polarization-independent characteristics in THz spectral region. At the same time, they experimentally demonstrated a MEMS reconfigurable digital metamaterial[24] for dynamic switching of THz anisotropy. In addition, Ho[25] presented a digitally reconfigurable binary coded THz metamaterial with the transmission output analogous to NOR and AND logic. However, these MEMS-based tunable devices are very complex, high cost, and difficult to fabricate.

*Project supported by the National Natural Science Foundation of China (Grant Nos. 61265005 and 11574059), the Natural Science Foundation of Guangxi, China (Grant Nos. 2015GXNSFDA19039 and 2014GXNSFAA118376), the Foundation from Guangxi Key Laboratory of Automatic Detection Technology and Instrument, China (Grant Nos. YQ14114 and YQ15106) and the Innovation Project of Guangxi Graduate Education, China (Grant Nos. 2016YJCX03 and 2016YJCX31).

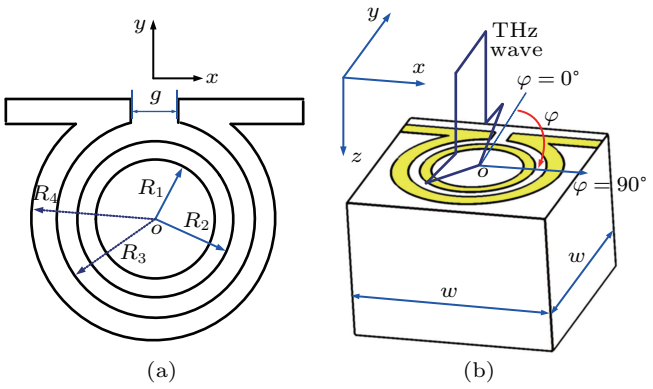
†Corresponding author. E-mail: hufangrong@sina.com

© 2017 Chinese Physical Society and IOP Publishing Ltd

In this paper, we experimentally demonstrated a mechanically tunable metamaterial THz dual-band bandstop filter. The filter consists of an inner aluminum circle and an outside aluminum Ohm-shape ring on the high-resistance silicon substrate. Two absorption peaks can be tuned by only rotating the sample along its normal axis. The sample is fabricated by a simple surface micromachining process, and the performance of the filter is simulated using a finite-integration-time-domain (FITD) method and experimentally demonstrated by a THz time-domain-spectroscopy (TDS) system. The physics mechanism for the tunability of each band is discussed and presented.

2. Design and fabrication

The unit cell of the filter is shown in Figs. 1(a) and 1(b). It is a square and composed of an inner aluminum circle and an outside aluminum Ohm-ring on the high-resistance silicon substrate. The structure parameters illustrated in Figs. 1(a) and 1(b) are radius $R_1 = 16$ μm, $R_2 = 20$ μm, $R_3 = 24$ μm, $R_4 = 30$ μm, gap $g = 8$ μm, and length of side $w = 74$ μm, respectively. The thickness of the metallic layer is 0.1 μm, and that of the silicon substrate is 350 μm. The THz wave is normally incident to the surface of the filter, and the azimuth φ (see Fig. 1(b)) can be changed by rotating the sample along its normal axis z.



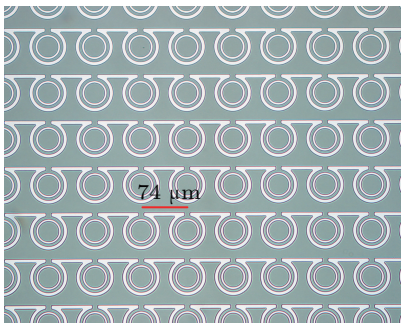


Fig. 1. (color online) Schematic of the sample: (a) top view, (b) oblique view of a unit cell, and (c) micrograph of sample.

The sample is fabricated using a surface micromachining process. Firstly, a layer of photoresist is used to form the Ohm-ring and circle structure. After the process of ultraviolet exposure and developing, the Ohm-ring and circle pattern are formed on the high resistance silicon substrate, and then a layer of aluminum film is deposited on the surface. Lastly, a lift-off process is used to form metal Ohm-ring and circle structure. The micrograph of the fabricated sample is shown in Fig. 1(c).

3. Simulation and experiment

In order to study the relationship between the structural parameters and the absorption peaks of the tunable filter, we simulated the filter with different structure parameters using FITD method. The simulation is implemented using the commercialized full-wave EM simulation software CST Microwave Studio 2015.[26] In the simulation, the y-polarized (azimuth $\varphi = 0°$) THz wave is normally incident to the surface of the sample. Open boundary condition was set in the z direction, and the unit cell boundary condition was set in the x and y directions, respectively. The metallic layer was modeled as lossy metal with an electric conductivity[26] $\sigma = 3.47 \times 10^7$ S/m. The high resistance silicon substrate is modeled as normal material[26] with an epsilon $\varepsilon = 11.9$ and a constant electrical conductivity $\sigma = 0.004$ S/m. When $R_4 = 30$ μm and $R_3 = 24$ μm, the transmission spectra of inner circles with different dimensions are compared in Fig. 2(a). For $R_2 = 20$ μm and $R_1 = 16$ μm, the transmission spectra of the outside Ohm-ring with different dimensions are plotted in Fig. 2(b).

Figure 2(a) shows that the low-frequency absorption peak is approximately independent of the radius of the inner circle, while the high-frequency absorption peak shows distinct redshift with the increase of the radius of inner circle. However, figure 2(b) shows that both of the absorption peaks are affected by the radius of the outside Ohm-ring. When the radius of the outside Ohm-ring increases, the low-frequency absorption peak shows distinct redshift, but the high-frequency absorption peak only produces a little blueshift. Therefore, the initial absorption peaks of the filter can be accurately tuned by changing its structural parameters.

The sample is characterized using a THz TDS system (Z-3, produced by Zomega Corporation). The experiment set-up is illustrated as Fig. 3, where QWP is quarter wave plate, WP is Wollaston prism, and PD is photodetector. The sample is placed on a rotatable metal holder with a central hole. A femtosecond laser (central wavelength is 780 nm) beam is divided into two beams by a beam splitter. One strong beam with the power of 110 mW is focused on the photoconductive antenna to generate THz pulse. The THz pulse passes through the sample and then reaches the ZnTe crystal. The other weak beam with the power of 18 mW is used as probe pulse, and it gets to the ZnTe crystal after passing through the optical delay line

and splitter. After transmitting through the QWP, the polarization of the probe pulse is changed due to the modulation of THz beam. The probe pulse continues to pass through a WP and then separates into two different polarization beams. The difference current produced by the PD is amplified by a lock-in amplifier and finally processed by the computer.

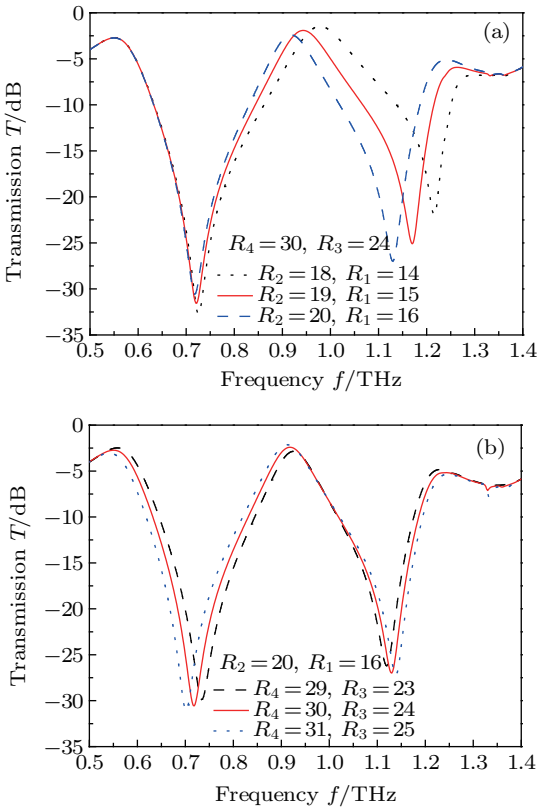


Fig. 2. (color online) Transmission spectra of the filter with different dimensions of inner circle (a) and outside Ohm-ring (b).

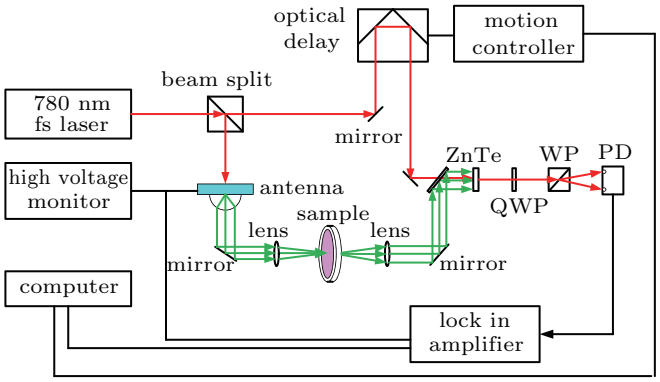


Fig. 3. (color online) Schematic of the experiment set-up.

For the filter with structural parameters detailed in Section 2, the simulations are shown in Figs. 4(a) and 4(b), and the experimental results are illustrated in Figs. 4(c) and 4(d), respectively. Figure 4 shows that, when the azimuth $\varphi = 0°$, two strong absorption peaks locate at about 0.71 THz and 1.13 THz, respectively. When the sample rotates anticlockwise along its normal axis and the azimuth φ increases from 0 to 90°, the high-frequency absorption peak gradually increases from 1.13 to 1.2 THz, while the low-frequency absorption peak (at 0.71 THz) gradually changes from bandstop to transparent with the increasing of azimuth φ. The experiment shows good agreement with the simulation. The probable reason for minor difference between experiment and simulation is that the THz wave is normally incident to the surface of the sample in the simulation, while it is focused on the top surface of the sample in the experiment.

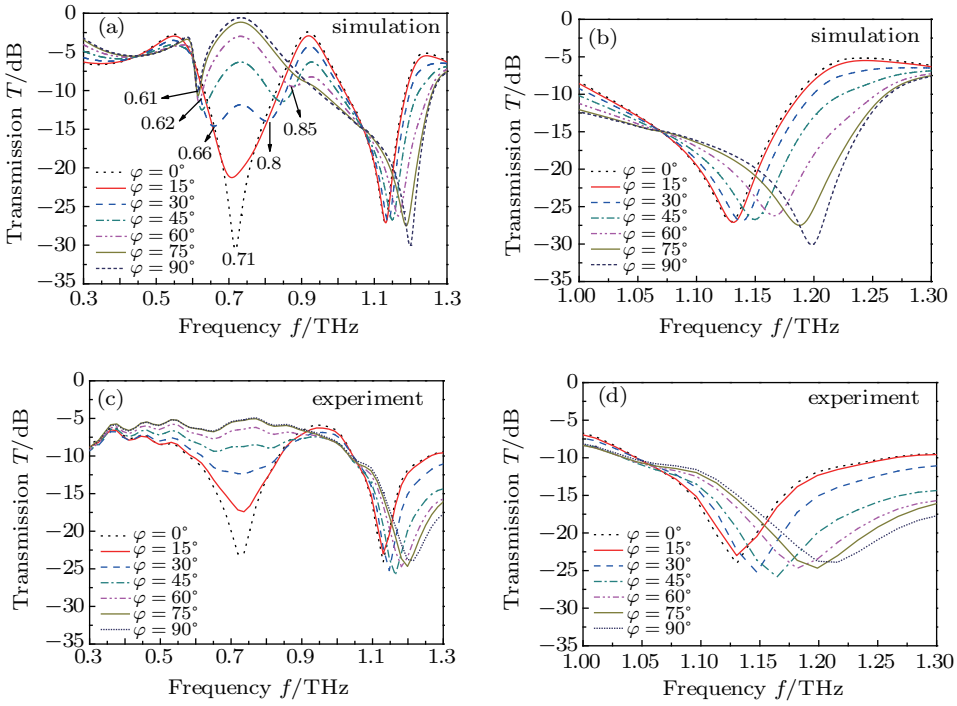


Fig. 4. (color online) Transmission spectra at different azimuth φ for simulation ((a), (b)) and for experiment ((c), (d)).

4. Physics mechanism

In order to investigate the physics mechanism of two absorption peaks and their tunable performance, we calculated the surface currents and electric fields of two absorption peaks.

1) High-frequency absorption peak

The transmission spectrum of a single inner circle is shown in Fig. 5(a), which indicates that the transmission spectrum is independent of the azimuth φ and the high-frequency absorption peak is just produced by current's resonance on the inner circle. For high-frequency absorption peak (f = 1.13 THz), surface current distributions at different azimuth, i.e., $\varphi = 0$, 30, 60, and 90°, are calculated using FITD method and shown as Figs. 5(b)–5(e), respectively. At the same time, the corresponding distributions of electric fields are also simulated and illustrated in Figs. 5(f)–5(i).

Figure 5 shows that the surface currents and the electric fields at high frequency are mainly distributed and oscillated on the inner circle, and thus two electrical dipoles are formed. This means that the high-frequency absorption peak is produced by the resonance of electrical dipoles on the inner circle. Based on electromagnetic theory, each electrical dipole can be equivalent to an LC resonator[27] and its resonance frequency is given by

$$f = \frac{1}{2\pi\sqrt{L_e C_e}}, \tag{1}$$

where L_e is the equivalent inductance and C_e is the equivalent capacitance of each electrical dipole. For $\varphi = 0°$, two electrical dipoles are symmetrically distributed on both sides of the inner circle. When the azimuth φ increases, two electrical dipoles transfer clockwise with the azimuth φ. At the same time, the equivalent inductance L_e of two electrical dipoles gets shorter and shorter with the increase of azimuth φ, and achieves a minimum at $\varphi = 90°$. As a result, according to Eq. (1), the resonance frequency f increases with the azimuth φ and gets to a maximum at $\varphi = 90°$.

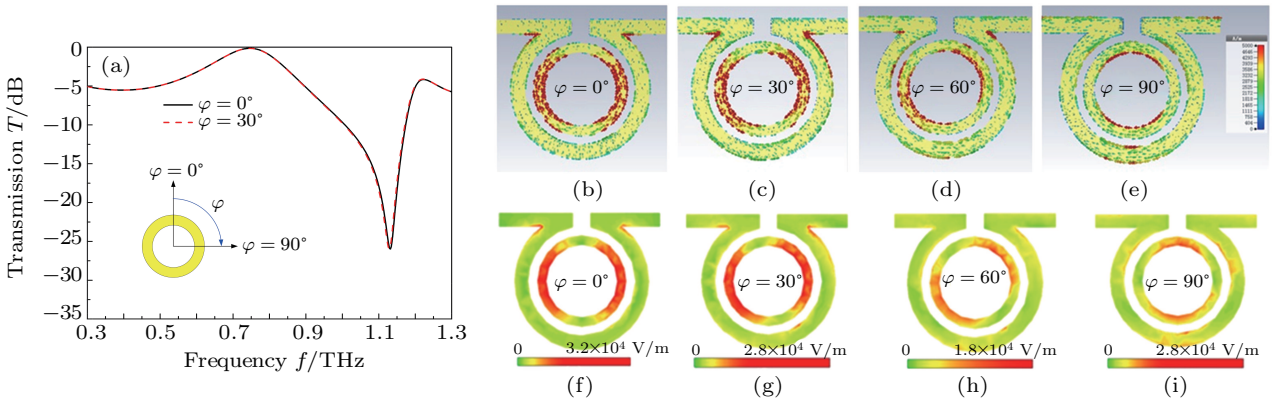


Fig. 5. (color online) Transmission spectrum of inner circle (a), surface current distributions at (b) $\varphi = 0°$, (c) $\varphi = 30°$, (d) $\varphi = 60°$, and (e) $\varphi = 90°$, and electric field distributions at (f) $\varphi = 0°$, (g) $\varphi = 30°$, (h) $\varphi = 60°$, and (i) $\varphi = 90°$.

2) Low-frequency absorption peak

In order to study the mechanism of the low-frequency absorption peak at f = 0.71 THz, the transmission spectra of the outer Ohm-ring at different azimuths are plotted in Fig. 6(a), which indicates that the outer Ohm-ring shows distinct polarization-dependent response. At the same time, the surface current distributions at $\varphi = 0$, 30, 60, and 90° are all calculated by FITD method and illustrated in Figs. 6(b)–6(g).

Figure 6(b) shows that the surface currents are mainly symmetrically oscillated on both sides of the outside Ohm-ring for $\varphi = 0°$. Very few image currents reversely distributed on the inner circle are excited by the electromagnetic induction between the inner circle and the outside Ohm-ring. Therefore, the low-frequency absorption peak at f = 0.71 THz (shown as Fig. 4(a)) is mainly produced by the resonance of surface currents distributed on the outside Ohm-ring.

Figure 6(c) indicates that when the azimuth φ increases to $\varphi = 30°$, some surface currents gradually transfer to the connecting arm of two neighboring unit cells. Thus, the effective length of the equivalent LC resonance will increase and the resonance frequency will shift from 0.71 THz to a low frequency, i.e., 0.66 THz (shown as Fig. 4(a)). At the same time, a high-frequency resonance mode, i.e., f = 0.8 THz (shown as Fig. 6(d)), will be excited, and the correspondingly resonance absorption peak at 0.8 THz emerges. As a result, the original resonance absorption peak at f = 0.71 THz will be gradually weakened, and the experimental result (shown as Fig. 4(c)) shows that the transmission magnitude changes from −23 dB to −13 dB. This effect is defined as rotationally induced transparent (RIT) which is dependent on the azimuth φ.

Figures 6(e) and 6(f) show that when the azimuth increases to $\varphi = 60°$, the length of surface current distribution will continue to increase. Thus, the low-resonance absorption peak will decrease to about 0.62 THz, and the high-resonance absorption peak will increase to about 0.85 THz.

Finally, figure 6(g) shows that the length of surface current distribution achieves a maximum at $\varphi = 90°$, and the corresponding resonance absorption peak at low frequency will get to a minimum of 0.61 THz.

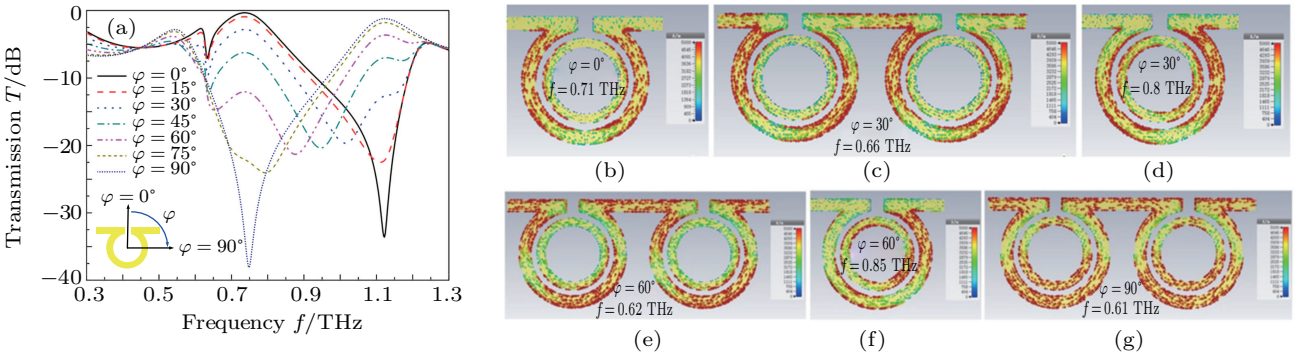


Fig. 6. (color online) Transmission spectrum of outer Ohm-ring (a) and surface current distributions at (b) $\varphi = 0°$, $f = 0.71$ THz, (c) $\varphi = 30°$, $f = 0.66$ THz, (d) $\varphi = 30°$, $f = 0.8$ THz, (e) $\varphi = 60°$, $f = 0.62$ THz, (f) $\varphi = 60°$, $f = 0.85$ THz, and (g) $\varphi = 90°$, $f = 0.61$ THz.

Therefore, when the azimuth φ gradually increases from 0 to 90°, the low frequency resonance absorption peak at 0.71 THz will change from bandstop to bandpass. At the same time, the effect of RIT will be gradually enhanced.

5. Conclusion

We experimentally demonstrated a mechanically tunable metamaterial THz dual-band filter composed of an inner aluminum circle and an outside aluminum Ohm-ring on the high resistance silicon substrate. The sample is fabricated using a simple surface micromachining process and characterized by a THz TDS system. The results show that when the incident THz wave is polarized in the y-axis, the filter has two intensive absorption peaks locating at 0.71 THz and 1.13 THz, respectively. When the sample rotates anti-clockwise along its normal axis, the high-frequency absorption peak shows distinct blueshift, while the absorption peak at low frequency gradually changes from bandstop to transparent due to the effect of RIT. Also, the filter is extremely flexible in which its operating frequency can be scaled by simply modifying the size of unit cell. Furthermore, this mechanically tunable filter has the advantages of simple structure, low cost, and easy fabrication, and thus it is very useful for switch, manipulation, and frequency selective detection of THz beam.

Acknowledgment

The authors acknowledge support from Prof. Weili Zhang and Dr. Ningning Xu of Oklahoma State University for their help with sample fabrication.

References

[1] Tonouchi M 2007 *Nat. Photonics* **1** 97
[2] Federici J F, Schulkin B, Huang F, Gary D, Barat R, Oliveira F and Zimdars D 2005 *Semicond. Sci. Tech.* **20** S266
[3] Wang S 2016 *IEEE Photonics Tech. L.* **28** 986
[4] Liu H B, Chen Y and Zhang X C 2007 *J. Pharm. Sci.* **96** 927
[5] Shen Y C and Taday P F 2008 *IEEE J. Sel. Top. Quant.* **14** 407
[6] Pendry J B, Holden A J, Robbins D J and Stewart W J 1999 *IEEE Trans. Microw. Theory Tech.* **47** 2075
[7] Bao D Shen X P and Cui T J 2016 *Acta Phys. Sin.* **64** 228701 (in Chinese)
[8] Sun X Y, Zheng L R, Li X N, Xu H, Liang X T, Zhang X P, Lu Y H, Lee Y P, Rhee J Y and Song W J 2016 *Chin. Phys. B* **25** 057802
[9] Alves F, Kearney B, Grbovic D and Karunasiri G 2012 *Opt. Express* **20** 21025
[10] Entezari M and Zavvari M 2016 *IEEE Sen. J.* **16** 8916
[11] Landy N I, Bingham C M, Tyler T, Jokerst N, Smith D R and Padilla W J 2009 *Phys. Rev. B* **79** 125104
[12] Ma Y, Chen Q, Grant J, Saha S C, Khalid A and Cumming D R 2011 *Opt. Lett.* **36** 945
[13] Tao H, Bingham C M, Pilon D, Fan K, Strikwerda A C, Shrekenhamer D, Padilla W J, Zhang X and Averitt R D 2010 *J. Phys. D-Appl. Phys.* **43** 225102
[14] Kuznetsov S A 2012 *Prog. Electromagn. Res.* **122** 93
[15] Teng C C, Zhou W, Zhuang Y Y and Chen H M 2016 *Acta Phys. Sin.* **65** 024210 (in Chinese)
[16] Ibraheem I A I, Jansen C, Born N and Koch M 2011 *Appl. Phys. Lett.* **98** 091107
[17] Zhang X Q, Gu J Q, Cao W, Han J G, Lakhtakia A and Zhang W L 2012 *Opt. Lett.* **37** 906
[18] Lu M Z, Li W Z and Brown E R 2011 *Opt. Lett.* **36** 1071
[19] Liang L J, Jin B B, Wu J B, Zhou G C, Zhang Y G, Tu X, Jia T, Jia X Q, Cao C H, Kang L, Xu W W and Chen J 2013 *Sci. China-Inform. Sci.* **56** 120412
[20] Ozbey B and Aktas O 2011 *Opt. Express* **19** 5741
[21] Fu Y H, Liu A Q, Zhu W M, Zhang X M, Tsai D P, Zhang J B, Mei T, Tao J F, Guo H C and Zhang X H 2011 *Adv. Funct. Mater.* **21** 3589
[22] Li Q, Zhang X Q, Cao W, Lakhatakia A, O'hara J F, Han J G and Zhang W L 2012 *Appl. Phys. A* **107** 285
[23] Pitchappa P, Ho C P, Qian Y, Dhakar L, Singh N and Lee C 2015 *Sci. Rep.* **5** 11678
[24] Pitchappa P, Ho C P, Cong L Q, Singh R, Singh N and Lee C 2016 *Adv. Opt. Mater.* **4** 391
[25] Ho C P, Pitchappa P and Lee C 2016 *J. Appl. Phys.* **119** 153104
[26] http://www.cst.com
[27] Ye Y Q, Jin Y and He S L 2010 *J. Opt. Soc. Am. B* **27** 498